



GLOBAL JOURNAL OF RESEARCHES IN ENGINEERING: J
GENERAL ENGINEERING

Volume 23 Issue 4 Version 1.0 Year 2023

Type: Double Blind Peer Reviewed International Research Journal

Publisher: Global Journals

Online ISSN: 2249-4596 & Print ISSN: 0975-5861

Creep Fatigue of Solder Joints in Electronic Assemblies

By E. H. Wong

Abstract- Electronic assembly is formed by mechanically joining, and hence electrically interconnecting, integrated circuit components onto printed circuit board using arrays of solder joints. Differential thermal expansion between the integrated circuit component and the printed circuit board leads to failure of solder joints through the combined mechanisms of creep and fatigue. This manuscript condenses the recent advances in creep fatigue analysis of solder joints in electronic assemblies into two major analyses: thermomechanical analysis and creep fatigue life modelling. The analytical thermomechanical analysis models an electronic assembly as a sandwich structure. By modelling the actual geometry of solder joints, it has found stout hourglass to be the ideal shape for solder joints that could reduce the magnitude of stress by 80% compared to the standard barrel-shape solder joints. The new creep integrated fatigue equation integrates the fundamental equation of creep into fatigue life equation and has been shown to model very well the creep fatigue of solder alloy.

Keywords: *thermomechanical analysis, environmental fatigue, optimum shape, life prediction, shear compliance.*

GJRE-J Classification: LCC: TK7871



Strictly as per the compliance and regulations of:



Creep Fatigue of Solder Joints in Electronic Assemblies

E. H. Wong

Abstract- Electronic assembly is formed by mechanically joining, and hence electrically interconnecting, integrated circuit components onto printed circuit board using arrays of solder joints. Differential thermal expansion between the integrated circuit component and the printed circuit board leads to failure of solder joints through the combined mechanisms of creep and fatigue. This manuscript condenses the recent advances in creep fatigue analysis of solder joints in electronic assemblies into two major analyses: thermomechanical analysis and creep fatigue life modelling. The analytical thermomechanical analysis models an electronic assembly as a sandwich structure. By modelling the actual geometry of solder joints, it has found stout hourglass to be the ideal shape for solder joints that could reduce the magnitude of stress by 80% compared to the standard barrel-shape solder joints. The new creep integrated fatigue equation integrates the fundamental equation of creep into fatigue life equation and has been shown to model very well the creep fatigue of solder alloy. More valuably, this methodology can be generalised to integrate general aggravating forces into fatigue life equation. It can be further generalised to integrate multiple aggravating forces into fatigue equation.

Keywords: thermomechanical analysis, environmental fatigue, optimum shape, life prediction, shear compliance.

I. INTRODUCTION

The mother board assembly constitutes morphologically the brain of an engineering device. The integrated circuits that are photolithographically etched onto silicon chips constitutes morphologically the brain cells. However, the brain cells on individual silicon chip are isolated from other chips; and they need to be electrically interconnected. The brain cells are very delicate and even the interconnects are mechanically fragile; and they need to be mechanically protected. Lastly, the brain cells generate high intensity of heat when running, and the heat needs to be dissipated before the brain cells would be burned. The jobs of electrical interconnection, mechanical protection, and thermal dissipation rest on the design and engineering of electronic and microelectronic assemblies [1].

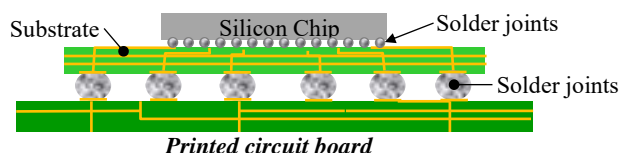


Figure 1: Schematic of the Cross-Section of an IC Component and a PCB

Figure 1 shows the schematic of a silicon chip that is electrically interconnected to a substrate, which is in turn interconnected to a printed circuit board, through arrays of solder joints. The former assembly is frequently referred to as an integrated circuit component/assembly while the latter is frequently referred to as a printed circuit board assembly. We shall refer to both assemblies as simply electronic assemblies. The solder joints are formed by melting solder balls/paste to form metallurgical bonds with the metal pads on the chip and the substrate, and with the metal pads on the substrate and the printed circuit board.

Electronic assemblies are susceptible to undue stress during manufacturing and while in service resulting in functional failure. In general, electronic assemblies may experience three main physics of damage: the violent vaporisation of the ingress moisture in the integrated circuit assembly during the solder joint forming process leading to cracking and/or delamination of the assembly [2][3]; fracturing of interconnection caused by drop-shock of mobile electronic products [2][4]; and lastly, creep-fatigue damage of interconnecting solder joints after repeated cycles of powering on/off of engineering devices [2][5]. The last is especially critical and has attracted maximum interest in

Author: e-mail: eehuawong@gmail.com

electronic assemblies. In essence, the differential thermal expansions between the silicon chip and the substrate and between the integrated circuit assembly and the printed circuit board give rise to cyclical deformation of the solder joints at temperature above their homologous temperature, driving them towards failure by the mechanism of creep fatigue. The propensity for creep fatigue failure of solder joints is aggravated by the trend towards increasing functionality of consumer electronic products, which is driving increase size of integrated circuit assembly and reduce size of solder joints.

The failure of a nuclear plant or a commercial aircraft is accompanied by unacceptable catastrophic consequences. The structural integrity and reliability of such products are therefore the paramount design considerations. In contrast, the two paramount design considerations for electronic assemblies are electrical performance and space. The former to support the ever-increasing performance of electronic products and the latter to support the increasing functionality of electronic products. Failure of consumer electronic products in service though annoying is acceptable to most users. This has encouraged a relatively relax attitude towards the structural integrity of electronic assemblies; and this is further encouraged by the relatively short life cycle of consumer electronic products. Nevertheless, there is a positive aspect of this more relax attitude towards structural analysis. The structural design of electronic assemblies is not bounded by a design protocol or a design code. Electronic assembly engineers are free to use any analysis method so long as the designed electronic assemblies will meet the integrity and reliability test requirements. It is inherently easy to monitor the structural integrity of an electronic assembly through monitoring the electrical connectivity of the assembly [6]. If necessary, the growth of damage in an electronic assembly can be tracked in real time through monitoring the changing electrical impedance of the assembly [6][7]. The absence of a strict design protocol and the ease of validating an analysis with tests has encouraged the exploration and adoption of new analysis methods, notwithstanding some of these methods may not be robust.

This manuscript gives a condensed presentation of the recent advances in the creep fatigue analysis of solder joints in electronic assemblies. This comprises two major analyses: thermomechanical analysis of solder joints in electronic assemblies; and creep fatigue life modelling of solder joints. It is believed that these advanced analyse techniques are fundamentally robust and they can be adopted to similar applications in other engineering field.

II. THERMOMECHANICAL ANALYSIS OF SOLDER JOINTS

Electronic assembly engineers routinely performed thermomechanical analysis of electronic assemblies using finite element analysis software in which the solder joints are modelled using solid finite elements. This has inadvertently led to singularity of stress/strain at discontinuities of geometry and materials giving rise to inconsistent analysis - because the magnitude of the stress/strain is dependent on the size and shape of the finite element at the site of singularity. To circumvent such singularity, electronic assembly engineers have adopted the practice of volume-averaging the stress/strain over a selected volume of solder joints [8][9]. Unfortunately, such arbitrary volume averaging act is equivalent to smearing the geometry of solder joints, effectively denying the engineers the ability to analyse the geometrical effects of solder joints on the magnitude of stress/strain. The issue of stress/strain singularity can be addressed by modeling the components of electronic assemblies as shells and beams. Maximum insights into the mechanics of the subject matter can be achieved through analytical modeling.

Analytical models of varied sophistication have been reported in the electronic assembling community [10][11][12][13]. In essence, an electronic assembly is treated as a sandwich structure constituting of array of solder joints sandwiched between two outer members. The simplest model treats the outer members as being infinitely rigid

and the solder joints as being infinitely compliant such that the solder joints experience only shear strain whose magnitude increases linearly with distance from the neutral plane of an electronic assembly and is given by $\gamma = \Delta\alpha T \cdot x/h$ (Figure 2a) [10], where $\Delta\alpha T$ is the differential thermal strain between the two outer members, x is the distance of a discrete joint from the neutral plane of the assembly, and h is the height of the discrete joint. This unrealistic model would grossly overestimate the magnitude of shear strain. The more sophisticated models treat the outer members as rectangular beams; and the solder joints as linear springs [11], or as cylindrical beams that are capable of shearing, flexing, and stretching [12][13]. The inclusion of elasticity of the outer members in the model have led to the vital understanding that shear strain in the solder joints does not increase linearly but exponentially with distance from the neutral plane of an electronic assembly. It takes the form $\gamma = \gamma_0 e^{\beta(x-l)}$ (Figure 2b), where γ_0 is approximately the shear strain at the outmost solder joint, β is a compliance parameter of the assembly, l is the half-length of the assembly.

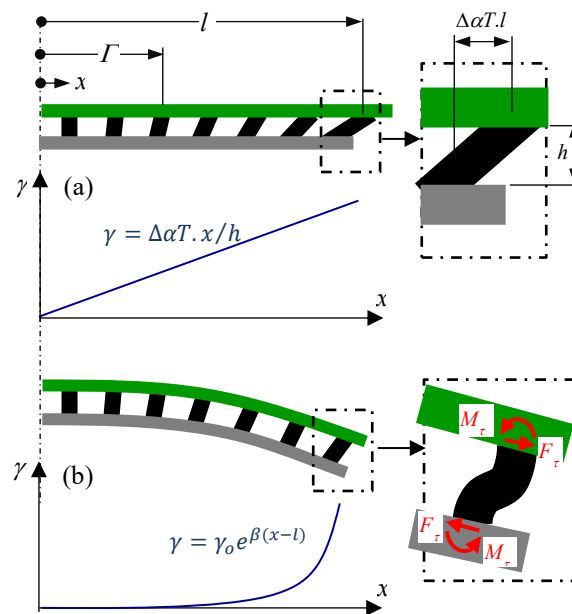


Figure 2: Analytical Models with Closed-Form Solution: (a) Infinitely Rigid Outer Members; (b) Outer Members as and Solder Joints as Elastic Beams

a) Analytical Modelling

Evaluating the stresses in the discrete joints of an assembly involves four steps of analysis, starting with smearing the discrete joints into a continuously bonded joint and then evaluating the compliances of the smeared assembly. This is followed by evaluating the smeared stresses in the smeared joints. The third step integrates the stresses into boundary forces and moments acting on individual discrete joint. The last step evaluates the stresses in the discrete joint due to the boundary forces and moments.

The discrete joints are assumed to be of identical shape and size and are distributed at uniform spacing. Figure 3 shows the schematic of discrete joints with a height h_d and spacing at pitches p_x and p_y along the x and the y coordinates, respectively. In the case that individual discrete joint is not of cylindrical shape but one with non-uniform sections along its height, it is represented by a pseudo cylindrical joints with a representative shear area, $A_{d,rep}$, and a representative second moment of area, $I_{d,rep}$, that would return identical shear and flexural stiffnesses as the original discrete joints [14]. These representative parameters are given by

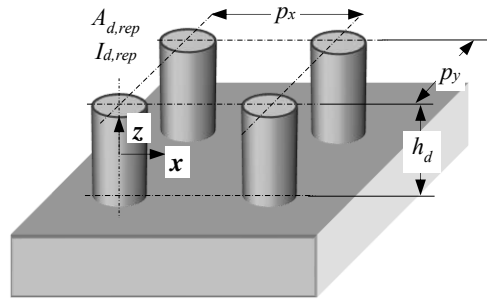


Figure 3: Schematic of Solder Joints

$$A_{d,rep} = \frac{1}{\int_{-h_d/2}^{h_d/2} \frac{dz}{A_z(z)}} \quad (1)$$

$$I_{d,rep} = \frac{1}{12 \int_{-h_d/2}^{h_d/2} \int_{-h_d/2}^z \frac{\xi d\xi}{I_z(\xi)} dz}$$

Referring to the outer members as member #1 and member #2, and the discrete joint as member #d, the height, the stretch modulus, the shear modulus, and the flexural stiffness of member #i are denoted as h_i , E_i , G_i , and D_i , respectively; the shear and the in-plane stretch compliances of the assembly are denoted as κ_s and λ_x respectively. For ease of reference, we shall refer to the moduli of the smeared joints as smeared moduli and the compliances as smeared compliances. Those characteristics that are associated with the smeared joints will be marked with an asterisk.

b) Compliances of a Smeared Assembly

The in-plane stretch compliance of the assembly is a function of the outer members and, for the case of plane stress, is given by [12][13]

$$\lambda_x = \sum_{i=1}^2 \left(\frac{1}{E_i h_i} + \frac{h_i^2}{4D_i} \right), \quad (2)$$

where in $D_i = E_i h_i^3 / 12$ for plane stress. The smeared shear compliance of the assembly, κ_s^* , is given by [12][13]

$$\kappa_s^* = \sum_{i=1}^2 \kappa_{si} + \kappa_{sd}^* + \kappa_{sd\phi}, \quad (3)$$

where

$$\kappa_{si} = \frac{h_i}{8G_i}, \quad \kappa_{sd}^* = \frac{h_d}{G_d^*}, \quad \kappa_{sd\phi} = \frac{h_d^3}{12D_d^*}. \quad (4)$$

wherein κ_{si} is associated with the shear compliance of member #i; κ_{sd}^* is associated with the shear deformation of the smeared joints; while $\kappa_{sd\phi}$ is associated with the flexural deformation of the discrete joints – referring to Figure 2b. The smeared shear modulus, G_d^* , and the smeared flexural rigidity, D_d^* , are given by $G_d^* = G_d A_{d,rep} / (p_x p_y)$ and $D_d^* = E_d I_{d,rep} / (p_x p_y)$.

c) Stresses in Smeared Joints

The shear stress in the smeared joints along the bonded length of a balanced assembly is given by [12][13][15][16]

$$\tau^*(x) = A_c^* e^{\beta^*(x-l)}, \quad x > 0, \quad (5)$$

where

$$A_c^* = \frac{\epsilon_T}{\sqrt{\lambda_x \kappa_s^*}} \quad (6)$$

$\beta^* = \sqrt{\lambda_x/\kappa_s^*}$; $\varepsilon_l = \Delta\alpha T$ is the differential thermal strain between the outer members.

d) Sectional Force and Moment in a Discrete Joint

The magnitude of the sectional shear force on a discrete joint that is at a distance Γ from the mid plane of the assembly may be evaluated approximately as

$$F_\tau(\Gamma) \approx \tau^*(\Gamma)p_x p_y, \tag{7}$$

The sectional shear force does not vary along the height of the discrete joint. On the other hand, and referring to Figure 4, rotational equilibrium dictates that the sectional moment varies linearly along the height of the discrete joint and is given by

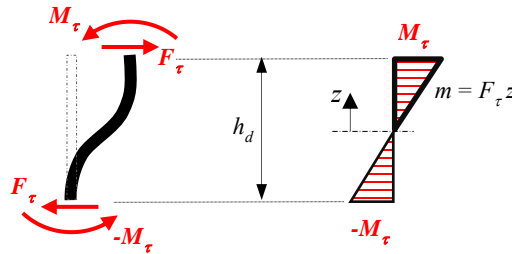


Figure 4: Bending Moment Distribution Along a Discrete Joint

$$m(\Gamma, z) = F_\tau(\Gamma)z, \tag{8}$$

where z is the local coordinate of a solder joint as shown in Figure 3.

e) Shearing and Bending Stresses in a Discrete Joint

The distribution of shear stress and bending stress along the height of a discrete joint, assuming it being an Euler beam, are simply [12][13]:

$$\begin{aligned} \tau_d(\Gamma, z) &= \frac{F_\tau(\Gamma)}{A_d(z)} \\ \sigma_b(\Gamma, z) &= m_\tau(\Gamma, z) \frac{r_d(z)}{I_d(z)} \end{aligned} \tag{9}$$

where $A_d(z)$, $I_d(z)$, and $r_d(z)$ are the local cross-sectional area, the local second moment of area, and the local outer fibre of the discrete joint. Assuming circular cross-section, as in the case of solder joints, the ratio r_d/I_d is reduced to $4/(\pi r_d^3)$. The largest magnitudes of shear force and bending moment, and hence shearing and the bending stresses, occur at the discrete joint furthest from the mid-plane of the assembly. Assuming $\Gamma_{max} = l$, these stresses are given by

$$\begin{aligned} \tau_{d,max} &= \frac{F_{\tau,max}}{A_{d,min}} \\ \sigma_b(l, z) &= \frac{4F_{\tau,max}z'}{\pi r_d^3(z)} \end{aligned} \tag{10}$$

where

$$F_{\tau,max} = \frac{\varepsilon_T p_x p_y}{\sqrt{\lambda_x \kappa_s^*}}, \tag{11}$$

and $A_{d,min}$ is the minimum cross-sectional area of the discrete joint.

f) *Optimum Shape of Solder Joints*

The solder joints are formed through controlled heating of solder into liquid form followed by controlled cooling the assembly to room temperature, forming metallurgical bonds with metal pads at its two ends. A solder joint will take up the natural shape of a spherical barrel, as shown in *Figure 5a*, that has the minimum surface energy. It is clear from Eq. (10) that a standard solder joint will experience the maximum magnitude of shear stress, $\tau_{d,max}$, and the maximum magnitude of bending stress, $\tau_{b,max}$, at its ends joining the outer members; and

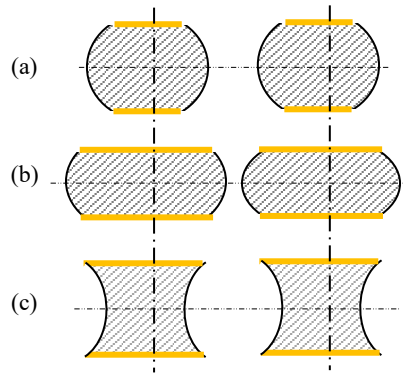


Figure 5: Geometries of Solder Joints (a) Barrel Shape, (b) Flatten Barrel Shape, (c) Stout Hourglass

$$\frac{\sigma_{b,max}}{\tau_{d,max}} = \frac{2h_d}{r_{d,end}} \tag{12}$$

where $r_{d,end}$ is the radius of the solder joint joining the outer member. In a standard barrel-shape solder joint, the magnitude of h_d is much larger than that of $r_{d,end}$. In other words, $\sigma_{b,max}$ is a far dominant stress in a standard barrel-shape solder joint. On paper, the magnitude of the dominant stress, $\sigma_{b,max}$, can be lowered by increasing the end radius of barrel-shape solder joints, which for the same volume of solder joint, will result in flatten barrel-shape solder joints leading to very significant reduction in the magnitude of $\sigma_{b,max}$. In practice, such a manipulation would inevitably raise the risk of bridging between adjacent solder joints, as is illustrated in *Figure 5b*.

It is clear from the linear distribution of bending moment in solder joints, as depicted in *Figure 4*, that solder joints should ideally have the shape of an hourglass. Solder joints of progressive hourglass shape can be designed into electronic assembly [14]. Modeling the curvature of an hourglass-shape solder joint as a hyperbolic sine curve and evaluating its representative shear area, $A_{d,rep}$, and representative second moment of area, $I_{d,rep}$, using Eq. (1), a stout hourglass-shape solder joint – similar to that illustrated in *Figure 5c* – has been found to return the minimum magnitude of stress for the same volume of solder as a standard barrel-shape solder joint. The maximum magnitude of bending stress, $\sigma_{b,max}$, in the stout hourglass solder joints is less than 15% that in a standard barrel-shape solder joints [14]. It is also worth noting that the use of stout hourglass solder joints does not increase the risk of bridging between solder joints.

III. CREEP FATIGUE MODELING

The fatigue life of a metal experiencing pure low cycle fatigue – that is, in the absence of aggravating element – and under a constant amplitude of cyclic stressing has been found to be satisfactorily modelled using the Coffin-Manson equation:

$$\epsilon_p = C_o N_f^{-\beta_o}, \tag{13}$$

where ε_p is the amplitude of the incremental plastic strain in a cycle; N_f is the number of cycles to failure; C_o and β_o are material dependent fitting constants. While it is tempting to extend the equation to creep fatigue modelling by replacing the plastic strain amplitude, ε_p , with inelastic strain amplitude, $\varepsilon_{in} = \varepsilon_p + \varepsilon_c$, wherein ε_c is the incremental creep strain in a single cycle, this simplicity approach of lumping creep strain with fatigue strain contradicts with the different macrostructural damages of creep and fatigue in metals [17][18] and has been convincingly disproved by abundant experimental data [19].

a) *A Brief Review of Practising Creep Fatigue Life Prediction Models*

The power generation community and the aerospace engineering community have vast knowledge and experience in modelling creep fatigue life of metals. Both the power generation and the aerospace communities have subscribed to the idea that creep fatigue damage can be evaluated by summing independently the damages due to creep, due to fatigue, and due to interaction of these two damages. The summative creep fatigue damage in a single creep fatigue cycle may be expressed mathematically as

$$d = d_f + d_c + d_{cf}. \tag{14}$$

Interestingly, the two communities have subscribed to different idea of defining the respective damages, d_f , d_c , and d_{cf} .

The aerospace community characterises the three cyclic damage indices from the hysteresis loop of a tension-compression creep fatigue experiment. Three components of inelastic strain: ε_{pp} , ε_{cc} , ε_{cp} (or ε_{pc}) are partitioned and extracted from the hysteresis loop, wherein the first letter of the subscript (c for creep and p for plastic strain) refers to the type of strain imposed in the tensile portion of the cycle, and the second letter refers to the type of strain imposed during the compressive portion of the cycle. Individual strain component is assumed to follow a power-law relation with the number of hysteresis cycles to failure. That is,

$$\varepsilon_{jk} = C_{jk} N_{jk}^{-\beta_{jk}}. \tag{15}$$

The damage per creep-fatigue cycle due to individual component is then simply

$$d_{jk} = \frac{1}{N_{jk}} = \left(\frac{\varepsilon_{jk}}{C_{jk}} \right)^{1/\beta_{jk}}. \tag{16}$$

This is known as the strain range partitioning model [19]. While this noble model has served the aerospace community well, its characterisation is inherently challenging.

The power generation community conveniently treats the cyclic fatigue damage, d_f , as that due to pure fatigue, which can be evaluated using the Coffin-Manson equation; that is,

$$d_f = \frac{1}{N_f} = \left(\frac{\varepsilon_p}{C_o} \right)^{1/\beta_o}; \tag{17}$$

and the cyclic creep damage, d_c , as that due to pure creep, which may be evaluated using the creep strain exhaustion rule:

$$d_c = \frac{1}{\varepsilon_R} \int_0^{t_c} \dot{\varepsilon}_c(t) dt, \tag{18}$$

wherein $\dot{\varepsilon}_c(t)$ is the instantaneous creep strain rate and t_c the cyclic period. However, the cyclic creep-fatigue interaction damage, d_{cf} , is a fitting index, which can only be established through extensive experimental characterisation [20][21][22].

The electronic packaging professionals have fallen for the creep fatigue equation of Darveaux [9],

$$N_{cf} = K_1 w_{in}^{K_2} \tag{19}$$

where $w_{in} = w_p + w_c$ is the sum of the cumulative plastic work density and the cumulative creep work density in a single creep fatigue cycle. Just like the failed idea of substituting plastic strain with inelastic strain in Eq. (13), the act of lumping the two work densities is clearly against the macrostructural evidence of the two damages. Consequently, and unsurprisingly, the fitting constants, K_1 and K_2 , are found to be dependent on the size and shape of individual electronic assembly [9], in other words, on the magnitude of the inelastic work density, w_{in} . Nevertheless, the electronic packaging community have stubbornly stuck with the model.

b) *Creep Integrated Fatigue Equation*

In the case of fatigue being the dominant mechanism in creep fatigue failure, the role of creep may be treated as one to lower the material capacity in fatigue. This has led to the idea of creep integrated fatigue equation [23][24][25]:

$$\varepsilon_p = C_o c(\varepsilon_p, T, t_c) N_{cf}^{-\beta_o}; \tag{20}$$

where $c(\varepsilon_p, T, t_c)$ is a function. Expressing the fatigue capacity in Eq. (13) for the case of pure fatigue as $\varepsilon_{p,ref}$ and it becomes clear that $c(\varepsilon_p, T, t_c) = \varepsilon_p / \varepsilon_{p,ref}$ describes the fractional fatigue capacity of a subject in the presence of creep. Its magnitude ranges from zero to unity - a zero magnitude corresponds to the case of pure creep while a magnitude of unity corresponds to the case of pure fatigue. The function $1 - c(\varepsilon_p, T, t_c)$ describes the fractional creep damage acting on the subject.

i. *The Fundamental Equations of Pure Creep In Metals*

The strain rate in a uniaxial steady-stress creep rupture experiment may be described in the form of Sherby-Dorn equation, $\dot{\varepsilon}_{SD}$, or Larson-Miller equation, $\dot{\varepsilon}_{LM}$, or Manson-Haferd equation, $\dot{\varepsilon}_{MH}$:

$$\begin{aligned} \dot{\varepsilon}_{SD} &= f(\sigma_s) e^{-H/kT}, T \geq 0 \\ \dot{\varepsilon}_{LM} &= B e^{-H(\sigma_s)/kT}, T \geq 0 \\ \dot{\varepsilon}_{MH} &= D e^{(T-T_{ref})r(\sigma_s)}, T \geq T_{ref} \end{aligned} \tag{21}$$

wherein $f(\sigma_s)$, $H(\sigma_s)$, and $r(\sigma_s)$ are functions of the applied tensile stress, σ_s ; k is the Boltzmann's constant; H , B , and D are material dependent constants; and T_{ref} is the temperature below which the mechanism of creep is assumed to be dormant. Assuming the dominance of the secondary stage of creep, the eventual creep rupture strain, ε_R , is given by

$$\varepsilon_R = \dot{\varepsilon}_{II} t_R, \tag{22}$$

where t_R is the time to creep rupture. Assuming ε_R to be independent of the applied stress and temperature, Eq. (21) may be rearranged into:

$$\begin{aligned} P_{SD}(\sigma_s) &= \frac{\varepsilon_R}{f(\sigma_s)} = \frac{t_R}{e^{H/kT}} \\ P_{LM}(\sigma_s) &= \frac{H(\sigma_s)}{k} = \frac{\ln t_R + \ln B_R}{1/T} \\ P_{MH}(\sigma_s) &= -\frac{1}{r(\sigma_s)} = \frac{T - T_{ref}}{\ln(t_R/t_\infty)} \end{aligned} \tag{23}$$

wherein $B_R=B/\varepsilon_R$ and $t_{\infty}=\varepsilon_R/D$. These functions are known respectively as the Sherby-Dorn parameter, the Larson-Miller parameter, and the Manson-Haford parameter. These parameters describe the relations between the applied stress, σ_s , and the gradient of the respective time-temperature function. These relations can be readily characterized and are used extensively in the creep rupture design of metal structures.

The corresponding stress parameter for a single stressing cycle may be expressed as [25]:

$$\begin{aligned} P_{c_SD}(\sigma) &= t_c e^{-H/kT} \\ P_{c_LM}(\sigma) &= T(\ln t_c + \ln B_c), \\ P_{c_MH}(\sigma) &= \frac{T-T_{ref}}{\ln(t_c/t_{c\infty})} \end{aligned} \tag{24}$$

where σ is the amplitude of the cyclic stress; and $B_c=B/\varepsilon_c$, $t_{c\infty}=\varepsilon_c/D$, and ε_c is the cumulative creep strain in a single cycle. Assuming (i) identical creep damage due to tensile and compressive stresses, and (ii) linear cumulation of creep strain over varied magnitudes of stress, then the cumulative creep strain in a single cycle may be expressed as $\varepsilon_c = \int_0^{t_c} k(|\sigma(t)|, T) dt$, where the function $k(|\sigma(t)|, T)$ represents one of the rate equations of the *SD*, *LM* and *MH*; and $|\sigma(t)|$ is the instantaneous magnitude of the cyclic stress. The cyclic stress parameter function may then be evaluated mathematically from the steady-stress parameter function as [25]

$$\begin{aligned} P_{c_SD}(\sigma) &= \frac{\phi_\varepsilon t_c}{\int_0^{t_c} \frac{dt}{P_{SD}(|\sigma(t)|)}} \\ P_{c_LM}(\sigma) &= \frac{\int_0^{t_c} P_{LM}(|\sigma(t)|) dt}{t_c}, \\ P_{c_MH}(\sigma) &= \frac{t_c}{\int_0^{t_c} \frac{dt}{P_{MH}(|\sigma(t)|)}} \end{aligned} \tag{25}$$

where $\phi_\varepsilon=\varepsilon_c/\varepsilon_R$.

ii. *Fractional Fatigue Capacity Function*

Let the fractional fatigue capacity function $c(\varepsilon_p, T, t_c)$ takes the form:

$$c(\varepsilon_p, T, t_c) = 1 - \chi(\varepsilon_p)\eta(T, t_c). \tag{26}$$

Herein $\chi(\varepsilon_p)\eta(T, t_c)$ is the fractional creep damage function. It is intuitive that the function $\eta(T, t_c)$ shall take the form of the rate equation of creep; that is,

$$\begin{aligned} \eta_{SD}(T, t_c) &= t_c e^{-H/kT} \\ \eta_{LM}(T, t_c) &= T(\ln t_c + \ln B_c), \\ \eta_{MH}(T, t_c) &= \frac{T-T_{ref}}{\ln(t_c/t_{c\infty})} \end{aligned} \tag{27}$$

It is worth noting that $\eta(T, t_c)$ vanishes at $T \leq 0$ for η_{SD} and η_{LM} and at $T \leq T_{ref}$ for η_{MH} when the mechanism of creep becomes dormant; the condition of pure fatigue prevails and the fractional fatigue capacity function $c(\varepsilon_p, T, t_c)$ acquires the maximum magnitude of unity. Similarly, the condition of pure creep requires that the magnitude of fractional fatigue capacity function vanishes to nil. This implies, from Eq. (24), that

$$X_k(\varepsilon_p) = \frac{1}{P_{c_k}(\sigma)}, \tag{28}$$

wherein the subscript k signifies *SD*, *LM*, and *MH*, respectively. The cyclic parameter function, $P_{c_k}(\sigma)$, can be evaluated from the steady-stress parameter function, $P_k(\sigma_s)$, using Eq. (25). Using the Ramberg–Osgood relation, $\sigma =$

$\bar{K}\varepsilon_p^{\bar{n}}$, where \bar{K} and \bar{n} are assumed to be the representative material constants over the range of temperature of interest, the cyclic parameters may then be expressed as a function of plastic strain; that is,

$$P_{c,k}(\sigma) \rightarrow P_{c,k}(\varepsilon_p). \tag{29}$$

The material dependent fitting constants, C_o , β_o , \bar{K} , \bar{n} , and ϕ_ε (the constant H may be evaluated from the steady-stress creep rupture test data) or B_c or $t_{c\infty}$, may be established through regressing the experimental creep fatigue data with Eq.(20). It is worth mentioning that the constants \bar{K} , \bar{n} , and ϕ_ε or B_c or $t_{c\infty}$ represent the damages due to pure creep and also creep fatigue interaction.

In practice, one can do away with the experimental characterisation of the steady-stress parameter function, $P_k(\sigma_s)$, and the subsequent mathematical evaluation of the cyclic parameter function, $P_{c,k}(\sigma)$. By expressing the steady stress parameter function as a power law in the form $P_k(\sigma_s) = p\sigma_s^q$, where p and q are fitting constants, it can be shown that the cyclic stress parameter function will be reduced to a power law function, $P_{c,k}(\sigma) = \hat{p}\sigma^{\hat{q}}$, where \hat{p} and \hat{q} are constants, for the sinusoidal and the triangular stress-time profile. This could then be transformed to $P_{c,k}(\varepsilon_p)$ using the Ramberg–Osgood relation. In other words, the function $\chi(\varepsilon_p)$ may simply be assumed to be a power-law function,

$$\chi(\varepsilon_p) = a\varepsilon_p^b, \tag{30}$$

where a and b are arbitrary constants. These two arbitrary constants can be established together with three material dependent fitting constants C_o , β_o , and H or B_c or $t_{c\infty}$, through regressing the experimental creep fatigue data with Eq. (20). This shall be illustrated in the following section.

iii. *Illustration and Validation*

The experimental creep fatigue data of Sn37Pb under cyclic triangular stress-time stressing generated by Shi et al. [26] has been analysed and the fitting constants, C_b and β_b , for nine sets of (ε_p, N_{cf}) data have been extracted and these are tabulated in **Table 1** [23]. Using these fitting constants, the (ε_p, N_{cf}) data were regenerated and these are depicted in *Figure 6*.

Table 1: Sn37Pb: Extracted Creep Fatigue Fitting Constants [23]

Creep-fatigue coefficients	Temperature (K) at $t_c = 1$ sec				
	233K	298K	348K	398K	423K
C_b	2.76	2.22	1.70	1.43	0.97
β_b	0.775	0.755	0.745	0.75	0.715
Creep-fatigue coefficients	Cycle time, t_c (s) at $T=298$ K				
	10^0 s	10^1 s	10^2 s	10^3 s	10^4 s
C_b	2.22	1.92	1.67	1.23	0.60
β_b	0.755	0.735	0.715	0.715	0.670

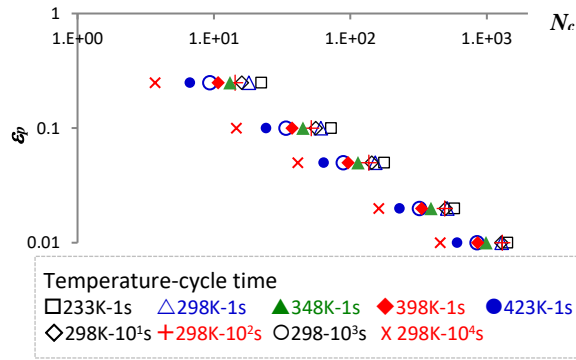


Figure 6: Sn37Pb: Regenerated Experimental Creep Fatigue Data

It is clear from Eq. (20) that a set of creep fatigue data, (ϵ_p, N_{cf}) , can be transformed into a set of pure fatigue data, $(\epsilon_{p,ref}, N_f)$, by transforming the magnitude of ϵ_p into $\epsilon_{p,ref}$ using the relation,

$$\epsilon_{p,ref} = \frac{\epsilon_p}{c(\epsilon_p, T, t_c)} \tag{31}$$

Let $c(\epsilon_p, T, t_c) = 1 - X_k(\epsilon_p)\eta_k(T, t_c)$, where $X_k(\epsilon_p) = a_k \epsilon_p^{b_k}$, the optimum values of C_o, β_o, a_k, b_k , and $H/k, B_c, t_{c\infty}$ corresponding to the three cyclic parameter functions have been established through regressing the transformed fatigue data $(\epsilon_{p,ref}, N_f)$ with the pure fatigue equation, $\epsilon_{p,ref} = C_o N_f^{-\beta_o}$. The optimum values are tabulated in **Table 2** completes with the relative magnitude of regression difference. The collapsed data of $(\epsilon_{p,ref}, N_f)$ corresponding to the three cyclic parameter functions are depicted in *Figure 7*.

Table 2: Sn37Pb: Fitting Constants for Creep Integrated Fatigue Equation Based on the Rate Equations of Sherby-Dorn, Larson-Miller, and Manson-Haferd

Rate equations	Fatigue coefficients		$\chi = a \epsilon_p^b$		Fitting constant for $\eta(T, t_c)$	Relative magnitude of regression residue
	C_o	β_o	a	b		
Sherby-Dorn	1.85	0.740	8.40×10^8	6.93×10^{-2}	$H/k = 8.98 \times 10^3$	3.4
Larson-Miller	6.58	0.806	1.17×10^{-4}	4.43×10^{-2}	$B_c = 4.39 \times 10^7$	2.8
Manson-Haferd	3.75	0.773	-2.00×10^{-2}	5.00×10^{-2}	$t_{c\infty} = 2.34 \times 10^7$	1

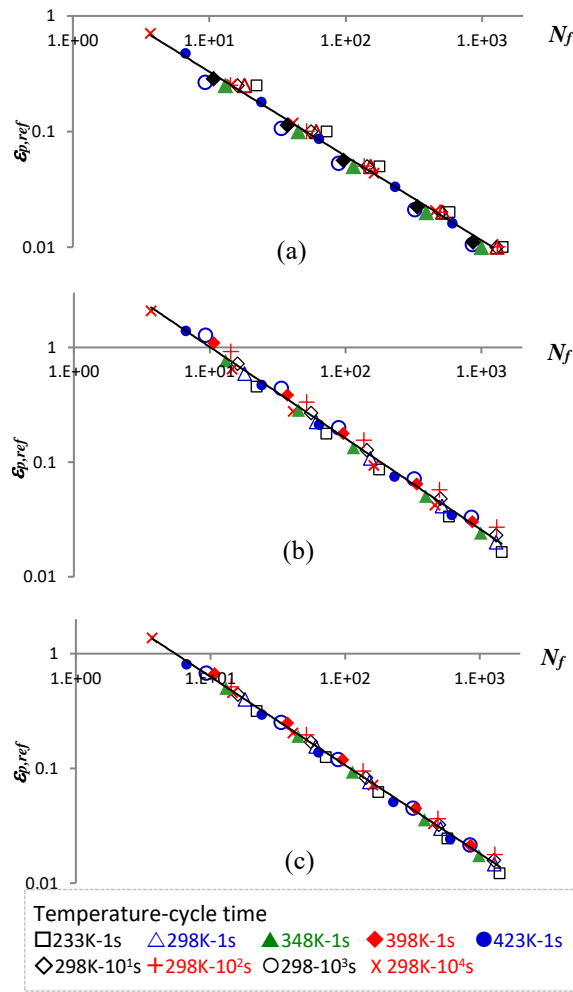


Figure 7: Sn37Pb: Transformed Pure Fatigue Data using the Rate Equations of (a) Sherby-Dorn, (b) Larson-Miller and (c) Manson-Hafred

It is noted that the fractional fatigue capability function that is based on the Manson-Hafred parameter returns a much smaller magnitude of regression residue than the other two parameter functions. This is consistent with the reported superior description of creep rupture of metal alloys for the Manson-Hafred parameter over the other two parameters [17]. Indeed, the magnitude of the fatigue capacity, C_o , given by the Sherby-Dorn parameter function was impossibly low – lower than the magnitude of C_b – while that given by the Larson-Miller parameter function appears to be unrealistically high.

IV. DISCUSSIONS

The creep integrated fatigue equation integrates seamlessly the damages of creep and fatigue over the range from pure creep to pure fatigue. Comparing to the approach of the damage summation method, the creep integrated equation offers a more cohesive account for the combined damages of creep and fatigue. It does away with the challenging characterisation experiment that is required for the strain range partitioning method.

More valuably, the method can be generalised to model metal fatigue that is aggravated by a generalised damage driving force, X , whose rate of growth of damage may be expressed in the form

$$\dot{x} = g(\mu)h(T, t), \tag{32}$$

where $g(\mu)$ is a function of the magnitude of the damage driving parameter (for example, $\mu \rightarrow \sigma$ in the case of creep being the damage driving force) while $h(T, t)$ is a function of temperature and time. The rate function, Eq. (32), shall then be expressed into the form:

$$\hat{g}(\mu)\hat{h}(T, t) = 1 \tag{33}$$

such as that shown in Eq. (23). The function $\hat{g}(\mu)\hat{h}(T, t)$ is the damage function for the damage driving force X . The damage force integrated fatigue equation is then given by

$$\varepsilon_p = C_o c(\mu, T, t_c) N_{xf}^{-\beta_o}, \tag{34}$$

wherein

$$c(\mu, T, t_c) = 1 - \hat{g}(\mu)\hat{h}(T, t_c). \tag{35}$$

The magnitude of $c(\mu, T, t_c)$ ranges from nil to unity corresponding to the case of pure fatigue and pure X damage, respectively. Let the damage function, $\hat{g}(\mu)$, takes the form $\hat{g}(\mu) = a\mu^b$, the fitting constants, C_o, β_o, a, b , and that associated with $\hat{h}(T, t_c)$ may be extracted through regression as illustrated in the previous section.

In case of a metal fatigue that is aggravated by n damage driving forces, Eq. (34) may be further generalised to integrate these damage forces, X_1, X_2, \dots, X_n , into the fatigue equation:

$$\varepsilon_p = C_o c_1(\mu_1, T, t_c) c_2(\mu_2, T, t_c) \dots c_n(\mu_n, T, t_c) N_{xf}^{-\beta_o}, \tag{36}$$

where

$$c_j(\mu_j, T, t_c) = 1 - \hat{g}_j(\mu_j)\hat{h}_j(T, t_c), \quad j=1,2,\dots,n, \tag{37}$$

and $\hat{g}_j(\mu_j)$ may be conveniently assumed to be a power law relation, $a_j\mu_j^{b_j}$. In the absence of interaction between the damage forces, the coefficients, a_j and b_j , of individual damaging force may be established individually by holding off other damaging forces.

It is worth mentioning that the Basquin equation, $\sigma = C_\sigma N_f^{-\beta_\sigma}$, may be substituted for the Coffin-Manson equation in Eq. (34) in the case of an environmentally aggravated high cycle fatigue situation.

V. CONCLUSIONS

Creep fatigue analysis of solder joints in electronic assemblies has been presented. The condensed presentation comprised two major analyses: thermomechanical analysis and creep fatigue life modelling. The advanced analytical analysis can optimize the geometry of solder joints to minimise the magnitude of stresses in solder joints. This has led to the ideal geometry of stout hourglass for solder joints. The creep integrated fatigue equation integrates cohesively the damages of creep and fatigue over the range from pure creep to pure fatigue. The methodology can be generalised to model metal fatigue that is aggravated by multiple damaging forces.

REFERENCES RÉFÉRENCES REFERENCIAS

1. Tummala RR (2001). Fundamentals of Microsystems Packaging, 1st edition, McGraw-Hill Education.
2. Wong EH & Mai Yiu-Wing, "Robust Design of Microelectronics Assemblies against Mechanical Shock, Temperature and Moisture, 1st Edition, Woodhead publishing, June 2015.
3. IPC/JEDEC-J-STD-020F (2023), Moisture/Reflow Sensitivity Classification for Non-hermetic Surface Mount Devices (SMDs)
4. JEDEC STANDARD JESD22-B111A (2016) Board Level Drop Test Method of Components for handheld electronic products.

5. JEDEC standard JESD22-A104-B (2000) Temperature Cycling.
6. Lamb MJ, Rouillard V, Sek MA, Monitoring the Evolution of Damage in Packaging Systems under Sustained Random Loads, Packaging technology and science, Volume25, Issue1 January/February 2012 Pages 39-51.
7. Kwon D, Azarian MH, Pecht M, Early Detection of Interconnect Degradation by Continuous Monitoring of RF Impedance, IEEE Trans. Device and Materials Reliability, Vol. 9, No. 2, June 2009.
8. Akay, HU; Paydar, NH; Bilgic, A. (1997). Fatigue life predictions for thermally loaded solder joints using a volume-weighted averaging technique. Journal of electronic packaging, 119, 228-235.
9. Darveaux, R. (2002). Effects of simulation methodology on solder joint crack growth correlation and fatigue life prediction. Trans. ASME J. Electron. Packag., 124, 147.
10. Engelmaier, W. (1983). Fatigue life of leadless chip carrier solder joint during power cycling. IEEE Trans on Components, Hybrids and Manufacturing Technology, 6, 232-237
11. Suhir E, "On a paradoxical phenomenon related to beams on elastic foundation: Could external compliant leads reduce the strength of a surface-mounted device?", J. Applied Mechanics, 55:818, 1988.
12. Wong EH & Wong CK (2008). Tri-Layer Structures Subjected to Combined Temperature and Mechanical Loadings. IEEE Trans. Comp. Packag. Techno., 31(4), 790-800.
13. Wong EH, Thermal stresses in the discrete joints of sandwiched structures, Comp Struct 2015;125:72-80.
14. Wong EH. Stout hourglass - the ideal shape for solder joints. Microelectronics Reliability 145 (2023) 114978.
15. Bigwood DA, Crocombe AD (1989). Elastic analysis and engineering design formulae for bonded joints. Int J Adhes Adhes, 9, 229.
16. Silva LFM et al. (2009). Analytical models of adhesively bonded joints—Part I: Literature survey, Int. J. Adhes. Adhes., 29, 319–330.
17. Penny, R. & Marriott, D. (1995). Design for creep (2nd ed.). Chapman & Hall.
18. Wong EH, Driel W. van, Dasgupta A., Pecht M., "Creep Fatigue of Solder Joints: A Critical Review", Microelectron. Reliab. 2016;59:1-12.
19. Manson, SS, Halford, GR, Hirschberg, MH (1971). Creep-fatigue analysis by strain range partitioning. Symposium on design for elevated temperature environment (pp. 12-28). New York: ASME.
20. AFCEN (1986). Design and construction rules for mechanical components of FBR nuclear island.
21. ASME (1988). Code Case N47-29, Class I components in elevated temperature service, Section III, Division 1. ASME.
22. British. (1991). The R5 procedures. Nuclear electric plc.
23. Wong EH & Mai Yiu-Wing, "A unified equation for creep fatigue", Int J Fatigue 2014;68:186-194.
24. Liu D., Pons D. & Wong EH, Creep-Integrated Fatigue Equation for Metals, Int. J. Fatigue 2016; doi.org/10.1016/j.ijfatigue.2016.11.030.
25. Wong EH. Derivation of novel creep-integrated fatigue equations. Int J Fatigue 128 (2019) 105184.
26. Shi XQ, Pang HLJ, Zhou W & Wang ZP (2000). Low cycle fatigue analysis of temperature and frequency effects in eutectic solder alloy. Int J Fatigue, 22, 217-228.

